Computers and Chemical Engineering 208 (2026) 109591

Contents lists available at ScienceDirect

Computers and Chemical Engineering

journal homepage: www.elsevier.com/locate/cace

Unlocking reactive power potential of industrial processes for voltage support through scheduling optimization

Philipp Glücker [a,b,c,*], Sonja H.M. Germscheid [a,c], Ariana Y. Ojeda-Paredes [a,c], Andrea Benigni [a,c,d], Manuel Dahmen [a], Thiemo Pesch [a]

[a] Forschungszentrum Jülich GmbH, Institute of Climate and Energy Systems, ICE-1: Energy Systems Engineering, Jülich 52425, Germany
[b] Department of Electrical and Electronic Engineering, The University of Melbourne, Melbourne, Victoria 3010, Australia
[c] RWTH Aachen University, Aachen 52056, Germany
[d] JARA-Energy, Jülich 52425, Germany

ARTICLE INFO

Keywords:
Ancillary services
Reactive power
Industrial process
Power flow
Scheduling optimization
Voltage stability

ABSTRACT

Demand response of industrial processes generally accounts for active power, but not reactive power which grows in importance for balancing local voltage levels in future electricity grids. We present an optimization-based approach to integrate reactive power into demand response scheduling and derive first estimates on the arising potentials. To this end, we extend a resource-task network scheduling model to account for the reactive power of electrically-powered process tasks, local power converters, and the local power grid. As an illustrative example, we study the multi-step copper production. We find a large achievable range of reactive power provision without compromising production volume or operating cost. Furthermore, we demonstrate how reactive power could be provided as an ancillary service by following a signal. Our results show that penalties or additional investment in compensation devices for power factor correction can be avoided through reactive power control of local power converters. Moreover, we demonstrate that industrial processes with sufficient capacity can alleviate voltage problems in transmission grids. Our work therefore lays the groundwork towards determining the reactive power scheduling potential of power-intensive production processes, and showcases its potential support for the voltage stability of future power grids.

1. Introduction

The energy transition leads to the decommissioning of conventional electricity generators and the expansion of renewable energy generation, which increases local imbalances between power supply and demand. In alternating current (AC) power systems, imbalances in the active power, i.e., the power that can be used to perform work, affect the system frequency, and are regulated by the transmission system operators (TSOs) by means of balancing reserves (Eicke et al., 2021). Imbalances in the reactive power, i.e., the non-working power responsible for the magnetic and electric fields, correlate with the local voltage level in the transmission grid. As reactive power transport over long distances should be avoided due to additional losses, reactive power compensation is required on a local level (Übertragungsnetzbetreiber, 2021). It is generally expected that in the future more reactive power provision will be needed to keep the local voltage levels within acceptable limits (Deutsche Energie-Agentur GmbH (dena) and TU Dortmund and ef.Ruhr GmbH, 2014). For instance, the current German network development plan for the year 2035 estimates that 26.4 Gvar of new controllable reactive power compensation devices must be installed (Übertragungsnetzbetreiber, 2021).

Nowadays, reactive power is primarily provided by conventional synchronous power plants which can adjust their reactive power generation (Plößer, 2021). This contribution is required by grid connection requirements that oblige these plants to provide reactive power within specified limits. Additional reactive power can be supplied through bilateral contracts with specific conventional power plants or through voltage-related re-dispatch, i.e., the adjustment of active power output to facilitate a change in reactive power, see, e.g., Next Kraftwerke (2023), Zhong and Bhattacharya (2002). Besides synchronous power plants, network resources of the TSOs can provide further reactive power, e.g., synchronous condensers, capacitor banks, high-voltage direct current (HVDC) converter stations, phase shifters, or on-load tap changers.

* Corresponding author at: Forschungszentrum Jülich GmbH, Institute of Climate and Energy Systems, ICE-1: Energy Systems Engineering, Jülich 52425, Germany.
E-mail address: p.gluecker@fz-juelich.de (P. Glücker).

https://doi.org/10.1016/j.compchemeng.2026.109591
Received 11 September 2025; Received in revised form 17 December 2025; Accepted 7 February 2026
Available online 9 February 2026

Nomenclature

Acronyms

AC	Alternating current
DC	Direct current
DR	Demand response
HVDC	High voltage direct current
IGBT	Insulated gate bipolar transistor
PCC	Point of common coupling
PF	Power factor
TSO	Transmission system operator

Latin symbols

b	Electric line susceptance
c	Electric line capacitance
g	Electric line conductance
N	Integer variable
P	Active power
p	Price
Q	Reactive power
R	Resource
r	Electric line resistance
S	Apparent power
V	Voltage
W	Square of voltage magnitude
x	Electric line reactance
y	Electric line admittance
z	Electric line impedance

Greek symbols

ϵ	Continuous variable
μ	Amount of consumed resources
ν	Amount of produced resources
Π	External in- and outflow
τ	Duration
θ	Power angle

Subscripts

i	Task
k	Electric bus
n	Electric bus
t	Discrete time step
aux	Auxiliary
el	Electric
est	Estimated

With the decommissioning of large conventional or nuclear power plants as part of the energy transition, alternatives for reactive power provision have to be identified. At the same time, power-intensive industrial plants are increasingly equipped with modern power converters for variable motor control (Straits Research, 2024). Leveraging these already installed power converters as distributed reactive power resources could complement or partly replace conventional, more expensive reactive power compensation devices. Currently, large electricity consumers such as power-intensive industrial production processes have to keep their reactive power demand within certain limits (Bundesnetzagentur, 2018), i.e., they are not incentivized to adapt their reactive power consumption to compensate for local imbalances in the grid. However, the idea that flexible industrial production processes could provide reactive power by adapting their operation has been discussed in recent years, see, e.g., Wolgast et al. (2022), Gesamtkonsortium NEW 4.0 (2021), Gesamtkonsortium NEW 4.0 (2021). Moreover, market-based systems are planned for the provision of reactive power, including a remuneration targeting the high-voltage grid (Blumberg et al., 2021; Federal Ministry for Economic Affairs and Climate Action Germany, 2023; Bundesnetzagentur, 2024).

Industrial process flexibility can be leveraged to optimize electricity consumption, i.e., by adjusting the production according to time-varying electricity prices, which is known as demand response (DR) (Daryanian et al., 1989). DR may help to reduce demand and supply mismatches, can reduce the electricity cost of a process, and is, for obvious reasons, particularly interesting for power-intensive processes (Albadi and El-Saadany, 2008; Vardakas et al., 2015; Zhang and Grossmann, 2016; Burre et al., 2020; Mitsos et al., 2018). Flexibility as an ancillary service is incentivized by various markets, see, e.g., Germscheid et al. (2023), Nolzen et al. (2022), Bohlayer et al. (2020). However, the existing works focus merely on leveraging active power. To the best of our knowledge, only the works by Plösser (Plößer, 2021) and Rauch and Brückl (Rauch and Brückl, 2023) consider the reactive power potential of small industrial loads and industrial compensation devices for the distribution grid. However, the work in Plößer (2021) is restricted to generic medium-voltage loads without process-level modeling, while Rauch and Brückl (2023) focus on static compensation devices and does not consider process flexibility. Importantly, neither of these two studies takes the operational complexity of industrial process scheduling into account. Bahl et al. (2017) and Baumgärtner et al. (2019) account for power inverters in their integrated design and scheduling of an energy system, but they do not study the ability of inverters to adjust reactive power.

DR of a process can be optimized by means of scheduling optimization, which seeks to alter the active power consumption of the process such that production cost are minimized while accounting for production and process constraints, see, e.g., Albadi and El-Saadany (2008), Vardakas et al. (2015), Zhang and Grossmann (2016), Burre et al. (2020), Mitsos et al. (2018). In principle, scheduling optimization could also account for the reactive power consumption and supply of individual process tasks and the power converters in the local, i.e., process internal, power grid, and thus enable reactive power provision. Reactive power scheduling of industrial processes, however, has not yet been described in the literature.

To bridge this gap, we propose to quantify the reactive power potential of a flexible power-intensive industrial production process using scheduling optimization. Specifically, we determine the difference between the maximum and minimum amount of achievable reactive power, and show how reactive power could be provided as an ancillary service by following an external signal. To this end, we consider the reactive power of key process tasks and account for the reactive power losses in the local electricity grid. We apply our approach to the copper production from our prior work (Röben et al., 2022) to showcase the evaluation of the reactive power potential of an industrial process for a specific example, and apply the identified reactive power potential to a simulation model of the German transmission grid.

The remainder of the paper is structured as follows: Section 2 introduces our approach for reactive power scheduling of power-intensive industrial processes which rests upon the power flow equations for modeling the internal electricity grid and few representative reactive power scheduling problems. In Section 3, we extend our previously published DR model of a copper production (Röben et al., 2022). In Section 4, we analyze the reactive power potential of the copper production and the ability of the process to follow an external reactive power signal. Moreover, we integrate the identified reactive power potential into a German transmission grid model and study the impact on local voltage stability. Section 5 discusses the results and presents the limitations of this study. Section 6 concludes our work.

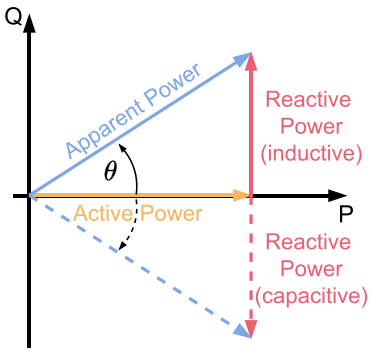

Fig. 1. Power triangle depicting the relation between active power (P), reactive power (Q), apparent power (S) and power angle (θ), adapted from Oeding and Oswald (2016).

2. Integration of reactive power into scheduling optimization

To integrate reactive power into process scheduling optimization, we consider the reactive power of individual process tasks (Section 2.1), the active and reactive power of the internal power grid (Section 2.2), and different reactive power-oriented scheduling objectives (Section 2.3).

2.1. Reactive power of process tasks

Electrical loads operating with AC power typically consume both active and reactive power. Fig. 1 depicts the so-called power triangle that shows the relation between the active power P, reactive power Q, apparent power S, and the power angle θ (Saadat, 1999). Here, the power factor

$$PF = \cos(\theta) = \frac{P}{S} = \frac{P}{P^2 + Q^2} \tag{1}$$

characterizes the ratio between active power and apparent power with a scalar value, i.e., $0 \leq PF \leq 1$, where lower values imply higher reactive power values relative to active power. As shown in Fig. 1, reactive power can be either inductive or capacitive. An inductive behavior suggests a lagging power factor, i.e., the current lags behind the voltage. In contrast, a leading power factor indicates capacitive behavior (Saadat, 1999). In the remaining paper, we refer to inductive behavior as *consuming* reactive power, and capacitive behavior as *supplying* reactive power, i.e., a negative sign for reactive power (Oeding and Oswald, 2016).

We account for the major electricity-consuming tasks of a process. In the present work, we assume a linear relationship between the active and the reactive power in the form of a fixed power factor to ensure an overall linear problem formulation for reasons of computational tractability of the scheduling optimization. Specifically, for a task i with fixed power factor $\mathrm{PF}_i = \cos\theta_i$ and respective power angle θ_i, the reactive power $Q_{i,t}$ at time step t depending on the active power $P_{i,t}$ can be determined as

$$Q_{i,t} = tan(\theta_i) P_{i,t}. \tag{2}$$

The fixed power factor modeling is employed for all process tasks that are not equipped with a power converter.

Power converters are electronic devices that transform electrical power between different forms, such as voltage waveform, voltage magnitude, or frequency (Mirafzal and Adib, 2020). In an industrial process, a task operating with direct current (DC) requires an AC-DC converter (Singh et al., 2004). Furthermore, AC-AC converters can electrically control, e.g., the speed or torque of motors (Finch and Giaouris, 2008). Although industrial loads are typically inductive, back-to-back converters, such as AC-DC and AC-AC converters, allow the grid-side current to be independently controlled, making capacitive operation technically feasible (Gao et al., 2021). By adjusting the phase shift between the current and voltage waveform characterized by the power angle θ, the power converters can flexibly consume or supply reactive power within thermal limits, i.e., the apparent power limitations of the connected lines, depending on the active power (Mirafzal and Adib, 2020; Kroposki et al., 2010). For simplicity, we assume a reactive power reference for the power converters, which in practice can be implemented via higher-level control, e.g., power factor targets or droop control (Akagi et al., 2017).

Often, specific details about the converter equipment of a particular process are lacking in the publicly available literature. In this work, we assume insulated gate bipolar transistor (IGBT) based power converters, which can control both active and reactive power (Mohan et al., 2002). In contrast, older converter types such as thyristor-based rectifiers cannot actively provide reactive power and typically rely on external reactive power compensation devices (Koponen et al., 2021; Ruuskanen et al., 2020). Due to their limited reactive power capability, these older converters are not considered in our study. For any process task i with a power converter, the reactive power $Q_{i,t}$ and the active power $P_{i,t}$ are limited by $S_{i,\max}$, i.e., the maximum apparent power of the power converter:

$$0 \leq P_{i,t}^2 + Q_{i,t}^2 \leq S_{i,\max}^2 \tag{3}$$

Following Naughton et al. (2021) and Naughton (2022), Eq. (3) can be linearized as follows:

$$P_{i,t} + Q_{i,t} \leq \sqrt{2} S_{i,\max}, \tag{4a}$$

$$P_{i,t} - Q_{i,t} \leq \sqrt{2} S_{i,\max}, \tag{4b}$$

$$0 \leq P_{i,t} \leq S_{i,\max}, \tag{4c}$$

$$-S_{i,\max} \leq Q_{i,t} \leq S_{i,\max} \tag{4d}$$

Note that the linearization can only be applied given that $P_{i,t} \geq 0$, meaning that active power is consumed and not produced by task i. This assumption is valid for converters attached to tasks that handle loads.

2.2. Power flow of internal power grid

The internal power grid refers to the on-site electrical network downstream of the point of common coupling (PCC), including the on-site substation at 110 kV and the medium- and low-voltage distribution grid. The PCC is the connection point between the internal power grid and the external superordinate transmission network. The power flow in the internal AC power grid must be modeled in order to account for the reactive power resulting from lines and transformers as well as the active and reactive power at the PCC. Note that for better readability, we disregard the time indices in the following power flow equations.

2.2.1. Exact AC OPF formulation

The AC optimal power flow (OPF) equations in the exact polar formulation read (Frank and Rebennack, 2016):

$$P_{nk} = g_{nk}|V_n|^2 - |V_n \parallel V_k|\big(g_{nk}\cos(\theta_n - \theta_k) - b_{nk}\sin(\theta_n - \theta_k)\big), \tag{5a}$$

$$Q_{nk} = b_{nk}|V_n|^2 - |V_n \parallel V_k|\big(g_{nk}\sin(\theta_n - \theta_k) - b_{nk}\cos(\theta_n - \theta_k)\big), \tag{5b}$$

$$|\underline{V}_n| \leq |V_n| \leq |\overline{V}_n|, \tag{5c}$$

$$P_{nk}^2 + Q_{nk}^2 \leq \overline{S}_{nk}^2 \tag{5d}$$

Here, $|V_n|$ denotes the voltage magnitude, P_{nk} and Q_{nk} are the active and reactive power transfer from bus n to bus k, respectively, and depend on the phase angle θ and account for the parameters line susceptance b_{nk} and line conductance g_{nk}. Eq. (5a) determines the active power transfer across the line between the electric busses n and k as a trigonometric function of the phase angles, voltage magnitudes, and line parameters. Similarly, Eq. (5b) defines the reactive power of the corresponding electric line. $\underline{V}_n$ and $\overline{V}_n$ in Eq. (5c) are the lower and

upper voltage magnitude limits, respectively. The voltage limits depend on the given regulatory framework and usually range between ±10 % of the nominal voltage (Forum Netztechnik/Netzbetrieb im VDE (FNN), 2013). $\overline{S}_{nk}$ denotes the apparent power limit for each line in Eq. (5d). Note that Eq. (5) is nonconvex and thus leads to computationally challenging optimization problems.

2.2.2. Linear distribution flow formulation

The linear distribution flow (LinDistFlow) equations are a linear lossless simplification of the AC power flow equations (cf. Eq. (5)) for radial medium- and low-voltage power grids (Low, 2014). We assume that industrial processes operate with a radial grid structure due to the simplicity and cost-effectiveness of such a structure (Love, 1993). The LinDistFlow equations are (Low, 2014):

$$\sum_{k:n\to k} P_{nk} = P_{jn} + P_n, \tag{6a}$$

$$\sum_{k:n\to k} Q_{nk} = Q_{jn} + Q_n, \tag{6b}$$

$$W_k = W_n - 2(r_{nk}P_{nk} + x_{nk}Q_{nk}), \tag{6c}$$

$$(\underline{V}_k)^2 \le W_k \le (\overline{V}_k)^2, \tag{6d}$$

$$|P_{nk}| + |Q_{nk}| \le \sqrt{2}\,\overline{S}_{nk}, \tag{6e}$$

$$\left[|P_{nk}|, |Q_{nk}|\right] \le \left[\overline{S}_{nk}, \overline{S}_{nk}\right], \tag{6f}$$

$$\text{with } z_{nk} = r_{nk} + \mathrm{j}x_{nk}, \tag{7a}$$

$$y_{nk} = \frac{1}{z_{nk}} = g_{nk} + \mathrm{j}b_{nk} = g_{nk} + \mathrm{j}2\pi f c_{nk} \tag{7b}$$

Eqs. (6a) and (6b) define the active and reactive power flow from bus n to bus k, respectively. Due to the radial structure of the network, bus n has one definite parent bus j and possibly multiple child buses k. Therefore, the power balance at bus n consists of the injected active power at bus n plus the active power flow from the parent bus P_{jn}, which equals the sum of active power flow to the child buses k. Eq. (6c) defines the voltage drops across lines using W_k, an auxiliary operational variable defined as $W_k = V_k^2$ with limits defined in Eq. (6d). In Eq. (6c), the voltage drop depends on the line resistance r_{nk} and line reactance x_{nk}. Eqs. (6e) and (6f) represent a linear approximation for the thermal limits of the cables and transformers based on Naughton (2022). Eqs. (7a) and (7b) define the line impedance z_{nk} and the line admittance y_{nk}, respectively, which allow to relate the line parameters b_{nk} and g_{nk} used in Eq. (5) to r_{nk} and x_{nk} used in Eq. (6) (Glover et al., 2017). In Eq. (7b), c_{nk} denotes the line capacitance, while j represents the imaginary unit and f is the grid frequency, e.g., 50 Hz.

We adopt the LinDistFlow equations in the scheduling optimization to ensure computational tractability. More accurate, nonlinear approximations of the AC power flow equations, e.g., the convex second-order cone programming (SOCP) approximation (Baradar et al., 2013), exist. However, preliminary investigations with the SOCP approximation have led to excessive computation time, thus we use the LinDistFlow formulation, aiming for an overall linear optimization model.

2.2.3. Integration of reactive power losses via linear regression

Reactive power losses in the internal power grid, particularly across transformers, are neglected in Eq. (6) but impact the overall reactive power potential at the PCC. Therefore, we augment the LinDistFlow equations with a linear regression model that determines Q_Δ, the estimated reactive power losses in the grid, with AC power flow simulations (cf. Eq. (5)) as described in Fig. 2.

The regression must take place before the actual scheduling optimization and needs representative operational data, e.g., data from preliminary scheduling that neglects or does not need Q_Δ. Representative schedules should include the active power P_{PCC} and the reactive power Q_{PCC} at the PCC based on realistic on/off decisions of individual process units, as these decisions impact the reactive power flows through the internal grid.

Table 1
Parameter values of the regression model (cf. Eq. (8)).

Parameter	Value	Unit
a	2.2512	Mvar
b	0.0297	–
c	0.0816	Mvar/MW

In Section 2.3, we set up and explain two scheduling problems in detail (see Eqs. (9) and (10)) that we use in the following to generate representative scheduling data for the linear regression. Note that for generating the data from Eq. (10), we neglect the linear regression by replacing $Q_{\mathrm{PCC,est},t}$ by $Q_{\mathrm{PCC},t}$ and removing the reactive power correction given by Eqs. (10d) and (10e). The resulting schedules represent diverse operating profiles of Q_{PCC} and the active and reactive power of the tasks. Using exact AC power flow (cf. Eq. (5)) simulation (Glücker et al., 2022), we can then determine the true reactive power $Q_{\mathrm{PCC,exact}}$ as well as the difference w.r.t. to Q_{PCC}, i.e., $Q_\Delta = Q_{\mathrm{PCC,exact}} - Q_{\mathrm{PCC}}$. This is followed by performing the regression step to determine the parameters a, b, and c needed to compute Q_Δ as a linear function of Q_{PCC} and P_{PCC}, i.e.,

$$Q_{\Delta,t} = a + b \cdot Q_{\mathrm{PCC},t} + c \cdot P_{\mathrm{PCC},t}. \tag{8}$$

Since the reactive power error depends on both active and reactive power, both variables are included in the approximation. Specifically, we use least squares regression from the *statesmodels* Python package (Seabold and Perktold, 2010), leading to the parameter values listed in Table 1. A visual comparison between the simulation data and the implemented linear approximation for Q_Δ is depicted in Fig. 3.

2.3. Scheduling problems

We now derive three scheduling problems with different objectives and slightly different constraints. Note that we use rather abstract representations of the overall optimization problems to focus on the main differences between the three problems.

First, we consider a conventional demand response scheduling optimization that aims for electricity cost minimization (Daryanian et al., 1989). This problem neglects reactive power and can be stated in brief as follows:

$$\min \quad \sum_t p_{\mathrm{el},t} \cdot P_{\mathrm{PCC},t} \tag{9a}$$

$$\text{s.t.} \quad P_{\mathrm{PCC},t} = \sum_{i\in\mathcal{I}} P_{i,t}, \tag{9b}$$

$$R_{\mathrm{limit}} \le \sum_t R_t, \tag{9c}$$

$$\text{Process model constraints} \tag{9d}$$

Here, the electricity costs depend on the electricity price $p_{\mathrm{el},t}$ and the active power consumption at the PCC, $P_{\mathrm{PCC},t}$, which are multiplied and then summed over all time steps t and shall be minimized. $P_{\mathrm{PCC},t}$ is the sum of the active power over all tasks $\mathcal{I}$ (cf. Eq. (9b)). Active power losses in the local power grid are neglected. Eq. (9c) accounts for a production constraint, i.e., the cumulative amount of product R must be greater than or equal to a minimum production limit R_{limit} at the end of the scheduling horizon. Note that R_{limit} can be determined prior to the demand response scheduling, e.g., by means of a production volume optimization (Röben et al., 2022), thus ensuring that reactive power provision does not compromise maximum production output. The process model constraints in Eq. (9d) include power intake constraints, storage and production constraints, and ramping constraints. The electricity consumption of individual process units is proportional to the production rate, which is enforced through the material balances and resource capacity constraints. Note that these process model constraints must be tailored to the specific process under consideration. For an

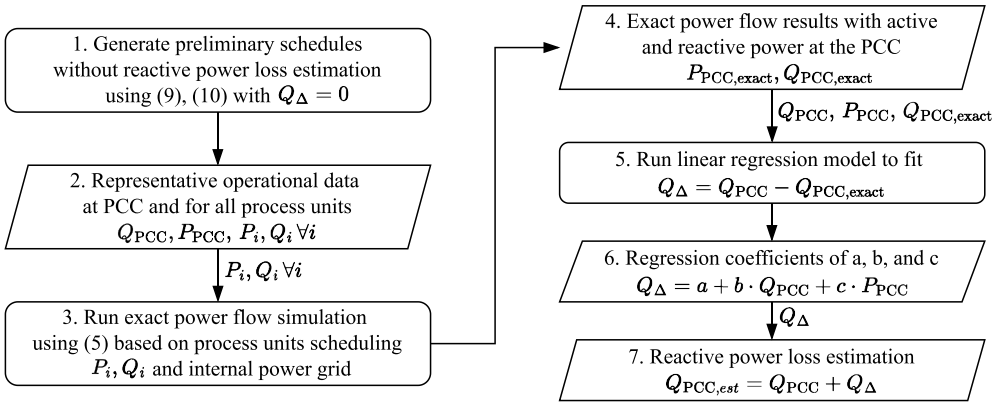

Fig. 2. Flowchart for determining the regression parameters a, b, and c for computing Q_Δ, the reactive power losses in the internal grid.

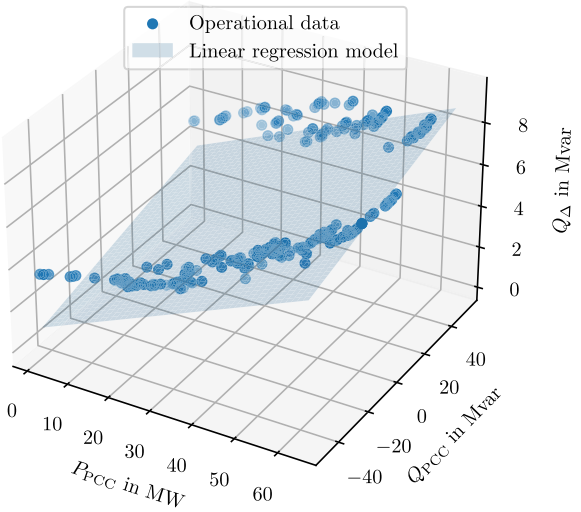

Fig. 3. Prediction of Q_Δ by the regression model (light blue plane) as a function of Q_{PCC} and P_{PCC} compared to the simulation data (blue dots) that was used for the calibration of the regression model.

example, we refer to our prior work on demand response scheduling of a copper production (Röben et al., 2022), which is briefly presented in Section 3.1.

Second, we formulate a scheduling problem that allows to determine the reactive power potential:

$$\max/\min \quad \sum_t Q_{PCC,est,t} \tag{10a}$$

$$\text{s.t.} \quad \text{LinDistFlow} \rightarrow P_{PCC,t}, \tag{10b}$$

$$\text{LinDistFlow} \rightarrow Q_{PCC,t}, \tag{10c}$$

$$Q_{\Delta,t} = a + b \cdot Q_{PCC,t} + c \cdot P_{PCC,t}, \tag{10d}$$

$$Q_{PCC,est,t} = Q_{PCC,t} + Q_{\Delta,t}, \tag{10e}$$

$$C_{limit} \geq \sum_t p_{el,t} \cdot P_{PCC,t}, \tag{10f}$$

$$R_{limit} \leq \sum_t R_t, \tag{10g}$$

$$\text{Process model constraints} \tag{10h}$$

Here, we either maximize or minimize the corrected reactive power at the PCC, aggregated over all time steps, i.e., we sum the momentary values over the scheduling horizon (cf. Eq. (10a)). Specifically, by subsequently maximizing and minimizing $Q_{PCC,est,t}$, we can quantify the available range of reactive power, i.e., the reactive power potential. Eqs. (10b) and (10c) describe the LinDistFlow model (cf. Eq. (6)) determining the active power $P_{PCC,t}$ and the reactive power $Q_{PCC,t}$ at the PCC. They are followed by Eq. (10d), i.e., the regression model for computing Q_Δ (cf. Eq. (8)), and Eq. (10e) for computing the corrected reactive power at the PCC, $Q_{PCC,est,t}$. We further consider a constraint Eq. (10f) that limits the allowable electricity cost. The cost limit C_{limit} can be based on the minimum electricity cost determined in a prior demand response optimization (cf. Eq. (9)), similar to the production volume constraint. This ensures that the reactive power potential is evaluated based on the cost-optimal schedule determined beforehand, i.e., Eq. (10f) ensures that providing reactive power does not incur additional electricity cost. Finally, the production volume constraint (10g) and the process model constraints (10h) are considered, identical to the demand response scheduling optimization depicted in Eq. (9).

Third, we consider the provision of reactive power as an ancillary service. Specifically, we assume that the industrial process shall follow an external reactive power signal, which can be written as

$$\min \quad \sum_t \left| Q_{PCC,est,t} - Q_{signal,t} \right| \tag{11}$$

$$\text{s.t.} \quad \text{Eqs. (10b)–(10h)},$$

which minimizes the absolute difference between the reactive power at the PCC $Q_{PCC,est,t}$ and an external reactive power signal $Q_{signal,t}$, aggregated over all time steps t. To obtain a linear formulation, we reformulate problem (11) as

$$\min \quad \sum_t Q_{aux,t} \tag{12a}$$

$$\text{s.t.} \quad Q_{aux,t} \geq Q_{PCC,est,t} - Q_{signal,t}, \tag{12b}$$

$$Q_{aux,t} \geq Q_{signal,t} - Q_{PCC,est,t}, \tag{12c}$$

$$\text{Eqs. (10b)–(10h)}, \tag{12d}$$

by introducing the auxiliary variable $Q_{aux,t}$.

3. Copper production as an illustrative example

As a specific application for determining the reactive power potential of a power-intensive industrial process, we consider the copper production based on our prior work (Röben et al., 2022). In the following, we briefly describe the process flowsheet, the modeling approach, and derive assumptions about appropriate power factors (Section 3.1) for the copper production. Subsequently, we conceptualize a possible internal power grid (Section 3.2), and explain the solution and evaluation procedure (Section 3.3).

3.1. Copper process model

The copper production is a multi-step production process whose flowsheet is shown in Fig. 4 (Schlesinger et al., 2011; Röben et al.,

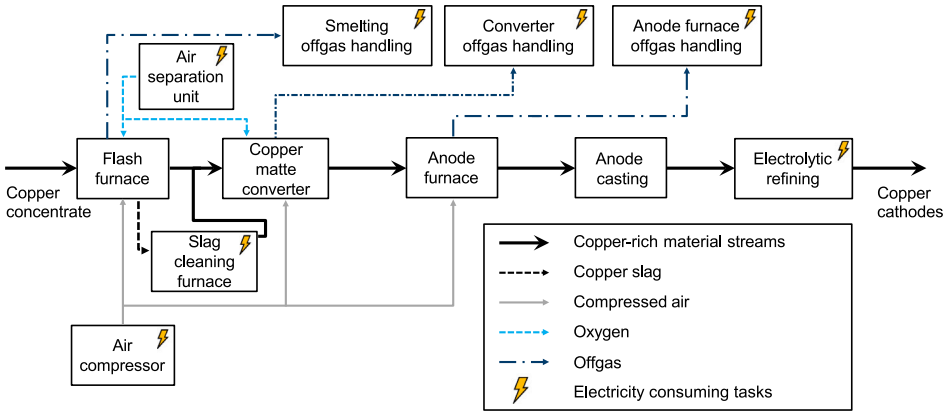

Fig. 4. Flowsheet of the copper production process: The copper concentrate is purified by various tasks resulting in cathode copper.
Source: The figure is adapted from Röben et al. (2022).

2022). Copper concentrate is turned into 99.99 wt-% copper by performing a sequence of continuous and batch tasks. Specifically, the copper concentrate is first melted and separated in a flash furnace. Iron and sulfur are then removed using the copper matte converter and anode furnace. Finally, the casted anodes are electrolytically refined.

Like in our prior work (Röben et al., 2022), we base the scheduling optimization model on a resource-task network (RTN) formulation (Pantelides, 1994) which is commonly used for scheduling of multi-step processes with both continuous and batch tasks, see, e.g., for steel plants (Castro et al., 2013) and cement plants (Castro et al., 2009). Note that while RTN formulations are capable of handling multi-product plants (Barbosa-Póvoa and Pantelides, 1997; Castro et al., 2005), the present work considers a single-product plant. In the RTN formulation, the resource balance

$$R_{r,t} = R_{r,t-1} + \sum_{i \in \mathcal{I}} \sum_{\theta_i=0}^{\tau_i} \left(\mu_{i,r,\theta} \, N_{i,t-\theta} + \nu_{i,r,\theta} \, \xi_{i,t-\theta} \right) + \Pi_{r,t}, \tag{13a}$$

with

$$R_{r,t}^{\min} \le R_{r,t} \le R_{r,t}^{\max}, \tag{13b}$$

$$V_i^{\min} N_{i,t} \le \xi_{i,t} \le V_i^{\max} N_{i,t} \tag{13c}$$

constrains the quantity of resource $R_{r,t}$ considering the resources $r \in \mathcal{R}$. $t \in \mathcal{T}$ denotes a time step. The resource amount $R_{r,t}$ is consumed or produced by the tasks $i \in \mathcal{I}$ or it is attributed to an external in- and outflow $\Pi_{r,t}$. A task i is associated with its specific duration τ_i, and the parameters $\mu_{i,r,\theta}$ and $\nu_{i,r,\theta}$ that specify the amount of consumed and produced resources, respectively. In particular, the integer variable $N_{i,t}$ and the continuous variable $\xi_{i,t}$ define the start and extent of the task, respectively. Eq. (13b) limits the resource by means of upper and lower bounds $R_{r,t}^{\min}$ and $R_{r,t}^{\max}$, respectively, e.g., to include storage constraints. Eq. (13c) constrains the rate of operation by means of the limits $V_i^{\min}$ and $V_i^{\max}$.

The RTN formulation does not explicitly define the active power consumption $P_{i,t}$ of a task i at time t, which is required for both the reactive power definitions (see Section 2.1) and the power flow in the internal power grid (see Section 2.2). Hence, we extend the RTN formulation by a definition for $P_{i,t}$, i.e.,

$$P_{i,t} = \sum_{\theta=0}^{\tau_i} \left(\mu_{i,P,\theta} \, N_{i,t-\theta} + \nu_{i,P,\theta} \, \xi_{i,t-\theta} \right). \tag{14}$$

Apart from Eq. (14), the process model follows the one from our previous work (Röben et al., 2022; Schlesinger et al., 2011), to which we refer for further details, most notably the specifications on the resources, tasks, and model parameters.

The major electricity-consuming tasks of the copper production are the air separation, the air compression, the electrolytic refining, the offgas handling, and the slag cleaning (Schlesinger et al., 2011). We distinguish between tasks that are driven by a motor and tasks that operate with a converter.

Tasks driven by electrical motors include the air separation, the air compression, and the offgas handling of the anode furnace. 90% of the power consumed by the air separation is for air-fed compressors that are driven by electrical motors (Kromer and Golubev, 2023; Aneke and Wang, 2015). The smelting section demands a significant amount of compressed air for the flash furnace, the copper matte converter, and the anode furnace (Röben et al., 2022). The air compressor uses electricity to operate its motors. The purification of the offgas of the anode furnace requires aspiration and passage through fans driven by electrical motors (European Commission, 2022). For all motor-driven tasks, we assume a fixed power factor of 0.88 as suggested by Cresswell (2009) for large industrial motors. While constant power factors do not capture voltage-dependent or time-varying reactive power behavior of real loads, a fixed power factor model is considered to maintain a linear problem formulation. For the slag cleaning, the electrodes in the furnace generate heat (Schlesinger et al., 2011). Although modern slag cleaning furnaces can run on DC (König et al., 2016), we consider an older furnace that runs on AC with a power factor of 0.93 (Barker and Stewart, 1980) to obtain a rather conservative estimate of the reactive power potential of the copper production. Table 2 summarizes the power factors.

Tasks equipped with a power converter include the electrolytic refining and the offgas handling of the flash furnace and the copper matte converters. The electrolytic refining requires electricity to drive the reaction and to maintain the operating temperature of the electrolysis cell. The cells require DC (Schlesinger et al., 2011), i.e., the task must be connected to the local AC grid via an AC-DC converter. In the offgas handling, sulfur dioxide is removed and a mechanical electrostatic precipitator removes dust from the gas stream (Schlesinger et al., 2011). The precipitator utilizes DC electrodes to create an electric field gradient (Schlesinger et al., 2011) and thus we assume an AC-DC converter for this task, too.

3.2. Power grid model

We assume a radial network, a common topology in medium-voltage and low-voltage networks (Abeysinghe et al., 2018; Love, 1993), allowing us to apply the LinDistFlow equations. If the internal network were meshed, the LinDistFlow approach would no longer be suitable, and a computationally more expensive OPF formulation would be required, accounting for reactive power and voltages. Within the internal radial network, we size the lines and the transformers such that they can handle the maximum possible apparent power to avoid line or transformer overloading. Furthermore, we assume that the internal power grid is connected to an external high-voltage network at 110 kV,

Table 2
The assumed power factors for the major electricity-consuming tasks of the copper production.

Task	Electricity-consuming component	Power factor	Power converter	Reference
Air separation	Motor-driven compressor	0.88	–	Kromer and Golubev (2023), Aneke and Wang (2015), Cresswell (2009)
Air compression	Motor-driven compressor	0.88	–	Kromer and Golubev (2023), Aneke and Wang (2015), Cresswell (2009)
Anode furnace offgas handling	Motor-driven fan/ventilator	0.88	–	European Commission (2022), Cresswell (2009)
Slag cleaning	Electrodes	0.93	–	Barker and Stewart (1980), Schlesinger et al. (2011), König et al. (2016)
Electrolytic refining	Electrolysis	–	AC-DC converter	Schlesinger et al. (2011)
Smelting & converter offgas handling	Electrostatic precipitator	–	AC-DC converter	Schlesinger et al. (2011)

Table 3
Voltage level assumptions and maximum active power of the tasks.

Task	Voltage level	Maximum active power (Röben et al., 2022)
Air separation	10 kV (VEM Motors Finland, 2021; Moore, 1974)	11.2 MW
Air compression	10 kV (VEM Motors Finland, 2021; Moore, 1974)	5.8 MW
Electrolytic refining	0.4 kV (Schlesinger et al., 2011)	15.2 MW
Slag cleaning	0.1 kV (Schlesinger et al., 2011)	3.0 MW
Smelting offgas handling	20 kV (Turner et al., 1988)	9.6 MW
Converting offgas handling	20 kV (Turner et al., 1988)	20.9 MW
Anode furnace offgas handling	0.4 kV (Unified Facilities Guide Specifications (UFGS), 2020)	1.7 MW

a common voltage level for the PCC between industrial processes and a superordinate grid (Ausfelder and Seitz, 2018).

We account for different voltage levels of the electricity-consuming process tasks which are taken from the literature (see Table 3). Based on the voltage levels, we create the radial topology of the internal power grid that is depicted in Fig. 5. We assume that the external network at 110 kV is connected to the process via two local transformers at 20 kV and 10 kV, respectively. The tasks operating at a lower voltage are connected via additional transformers down to 0.4 kV and 0.1 kV.

Table 3 lists the maximum active power of each task, which allows us to derive the line and transformer parameters of the internal power grid which are listed in Table A.1 of Appendix A. The cables and transformers are based on standard values which can be found in the standard type library of *pandapower* (Thurner et al., 2018) for the respective voltage level. In cases where the maximum power of the electrical components is not sufficient, we assume a parallel arrangement of multiple components, leading to an increased apparent power. Note that the values given in Table A.1 are absolute values of the resistance R_{nk}, the reactance X_{nk}, and the capacitance C_{nk}. They can be converted to the per-unit system used in Eqs. (5), (6), (7a) and (7b) via

$$r_{\mathrm{nk}} = R_{\mathrm{nk}} / Z_{\mathrm{base}}, \tag{15a}$$

$$x_{\mathrm{nk}} = X_{\mathrm{nk}} / Z_{\mathrm{base}}, \tag{15b}$$

$$c_{\mathrm{nk}} = C_{\mathrm{nk}} / Z_{\mathrm{base}}, \tag{15c}$$

with Z_{base} representing the assumed base impedance of 100 Ω. For further information on the per-unit system, the reader is referred to Frank and Rebennack (2016), Glover et al. (2017).

3.3. Solution and evaluation approach

The scheduling problems (9), (10), and (12) are mixed-integer linear programs (MILPs), with the integer variables indicating the startup decisions of the process units. To determine the production volume and electricity cost limits appearing in these problems, we perform a production volume maximization and an electricity cost minimization prior to the scheduling, following our previous works (Röben et al., 2022; Germscheid et al., 2023). To estimate the reactive power losses Q_{Δ} in the internal grid ahead of the actual scheduling optimization, we first derive a linear approximation following the procedure described in Section 2.2.3. This linear power flow model is then incorporated into all scheduling optimizations. Finally, based on the determined schedule, the exact active and reactive power at the PCC is computed through a nonlinear power flow simulation (Glücker et al., 2022) during post-processing.

All scheduling optimizations are performed on a 1.8 GHz Intel Core i7-1265U CPU with 32 GB of RAM using Gurobi 11.0.2 (Gurobi Optimization, LLC, 2024). The MIP gap is set to 1 %. We assume 5% oversizing for the power converters, i.e., we set the maximum apparent power of a power converter to $S_{i,\max} = 1.05 \cdot P_{i,\max}$ in Eq. (3) with $P_{i,\max}$ according to Table 3. In the following presentation of results, we show the exact reactive power at the PCC as determined by the AC power flow equations.

4. Results

For the assessment of the reactive power potential of the copper production, we consider three different operating strategies: scheduling neglecting reactive power (Section 4.1), scheduling evaluating the achievable range of reactive power (Section 4.2), and scheduling following an external reactive power signal (Section 4.3). In Section 4.4, we evaluate the impact of the reactive power provision on the German transmission grid. To this end, we use a simulation model of the German electricity system from our prior work (Pesch, 2019) which integrates a detailed model of the European electricity market and the German transmission grid.

4.1. Scheduling neglecting reactive power

We first consider an operation of the copper production that solely accounts for active power and thus neglects the reactive power in the scheduling optimization. Specifically, we consider the optimization problem Eq. (9) that minimizes the electricity cost.

The active power demand, reactive power demand, and the resulting overall power factor of the process are depicted for the cost-optimal schedule in Fig. 6. Note that for tasks with converters (cf. Table 2), we assume a power factor of 1 in the evaluation of the schedule, i.e., reactive power is neither produced nor consumed by the respective task. As intended, the active power demand is lower when electricity prices are high and higher when prices are low. As a consequence of the fixed power factors, the reactive power demand is generally similar to the active power demand. However, due to the varying operation of the tasks with different power factors, the overall power factor varies between values of 0.92 and almost 1. Occasionally, the

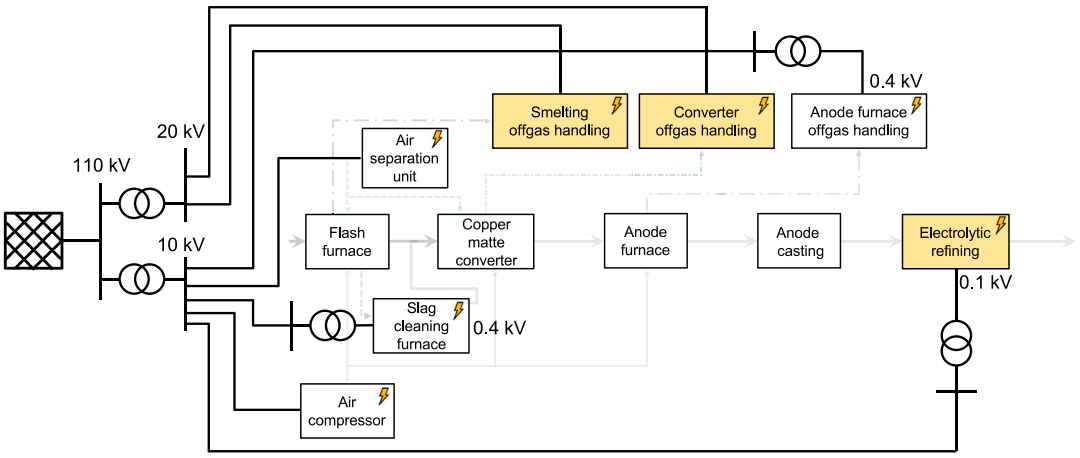

Fig. 5. Internal power grid of the copper process with radial network structure. The tasks highlighted in yellow are tasks equipped with a power converter. The shaded/dashed lines represent the flow of the resources (see Fig. 4).

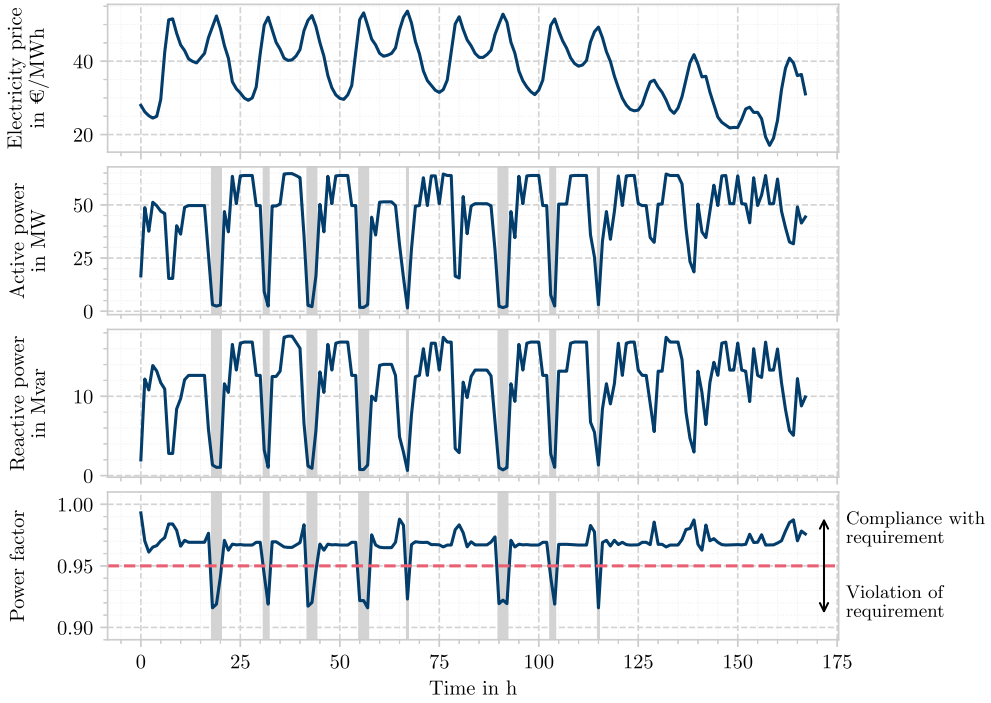

Fig. 6. Cost-optimal scheduling of the copper production neglecting reactive power and assuming a power factor of 1 for all power converters. The results are obtained from a nonlinear AC power flow simulation (Glücker et al., 2022), using the cost-optimal schedules as inputs: Electricity price profile (top), active power demand (top-center), reactive power demand (bottom-center), and power factor at the PCC (bottom). The gray areas indicate violations of a German grid connection requirement stating that the power factor at the PCC must not fall below 0.95 (Bundesnetzagentur, 2018).

power factor drops below the value of 0.95 which consumers connected to high voltage, e.g., industrial production processes, are required to maintain in Germany (Bundesnetzagentur, 2018). Such violation of grid requirements usually occurs during hours of rather low active power demand. As we show in Appendix B, during these times only the slag cleaning furnace with its power factor of 0.93 is operating. In combination with the reactive power consumption of the connecting low-voltage transformer, the process power factor drops slightly below 0.92. To avoid penalties by the TSO, local compensation devices such as capacitor banks would be installed (Peñalvo-López et al., 2021). These additional investment costs could be avoided by reactive power control of local power converters, as demonstrated in the following.

4.2. Evaluating the reactive power potential

We now assume that the local power converters (cf. Table 2) can be operated within the stated limitations of Eqs. (4a)–(4d) and thus constitute degrees of freedom with respect to reactive power provision in scheduling optimization. Specifically, we minimize and maximize the reactive power at the PCC while ensuring both maximum copper production and minimum electricity cost (cf. problem (10)).

Fig. 7 shows the resulting margin of reactive power which we define as the difference between the maximum and minimum obtained reactive power values at any given point in time and refer to as the reactive power potential of the process. Furthermore, minimum,

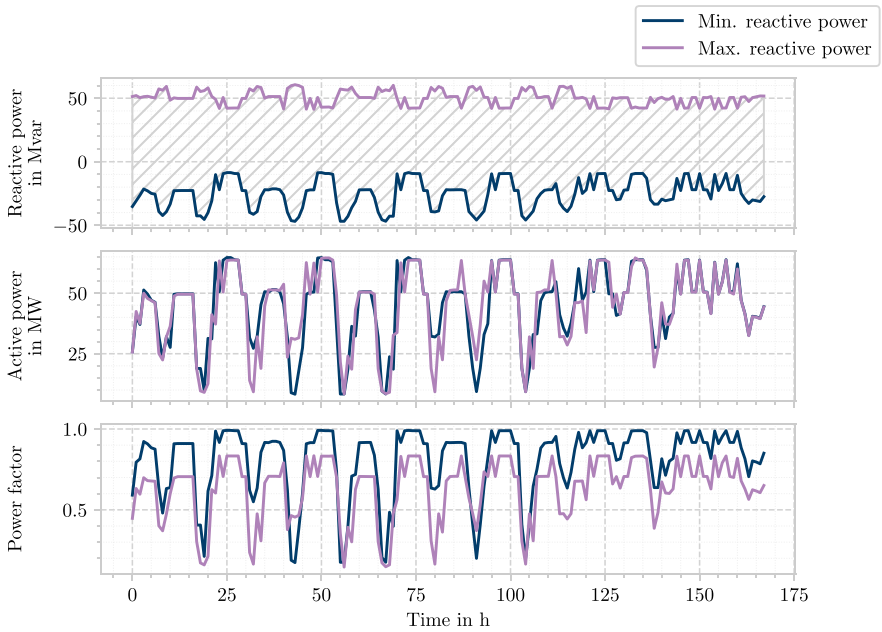

Fig. 7. Reactive power potential of the copper process: The minimum and maximum reactive power (top) are obtained from a nonlinear AC power flow simulation (Glücker et al., 2022), using the solved scheduling Eq. (10) as inputs. The hashed area corresponds to the reactive power potential. The active power (center) and power factor (bottom) corresponding to the minimum and maximum reactive power schedules are indicated. Note that the power factor for minimum reactive power (blue) always corresponds to capacitive behavior, and the power factor for maximum reactive power (purple) always corresponds to inductive behavior.

maximum, and average values for minimizing and maximizing the reactive power as well as the reactive power potential of the copper process are listed in Table 4. Note that a positive reactive power suggests that the industrial production process has inductive behavior, i.e., it consumes reactive power. In contrast, a negative reactive power indicates that the industrial production process has capacitive behavior, i.e., it produces reactive power. The range between capacitive and inductive power factors for each time step shows that with the reactive power control of local converters, penalties by the TSO or additional investment in compensation devices can be avoided without additional operating costs. In both Fig. 7 and Table 4, the absolute values of the maximum reactive power, i.e., the maximum consumed reactive power, are significantly higher than that of the minimum reactive power, i.e., the maximum produced reactive power. Converter-based tasks can both consume and produce reactive power. In contrast, the tasks with fixed power factors and the transformers always consume reactive power. Thus, the reactive power consumption is larger than the reactive power production. Furthermore, Fig. 7 and Table 4 reveal a significant reactive power margin suggesting a substantial potential for reactive power provision by the copper production.

In addition to the reactive power profile, Fig. 7 shows the active power profile and the resulting power factor. It reveals that the active power varies slightly for the schedules that maximize and minimize the reactive power, indicating different process operations (for further details see Appendix C of the supporting materials). Furthermore, it shows that the power factor can vary between 0.2 and 1, with the power factor associated with minimizing the reactive power indicating capacitive behavior, i.e., supply of reactive power, and the one associated with maximizing reactive power indicating inductive behavior, i.e., consumption of reactive power.

The identified average reactive power potential amounts to 72.1 Mvar (cf. Table 4). It can be related to the required new installations of reactive power compensation devices to stabilize the power grid. By 2035, Germany is projected to require additional 87 controllable reactive power compensation devices, each with an average size of 300 Mvar (Übertragungsnetzbetreiber, 2021). In approximate terms, four industrial processes of the size of the investigated copper production could replace one such compensation device. However, the total controllable reactive power compensation requirement of 26.4 Gvar for Germany is further divided into 25 regions, each with its own specific compensation needs (Übertragungsnetzbetreiber, 2021). The average reactive power potential of the copper process could meet about 2 % of the installation requirement in the region with the highest compensation requirement (region *D24* in central Germany), and up to 58 % in the region with the lowest compensation requirement (region *D77* in southwest Germany). Section 4.4 demonstrates the impact of the identified reactive power potential of the copper production on the voltage stability of the German transmission grid in region *D25* in southern Germany. In this region, around 5 % of the required reactive power compensation could be provided by the identified potential. Note that the presented reactive power potential constitutes a rather conservative estimate, as it considers power converters for DC-based process units only and not for AC-based units, which in principle could be equipped with AC-AC converters resulting in additional reactive power potential. For a more detailed assessment of the approximation error introduced by the linearized power flow approximation, we refer the reader to Appendix D.

We envision that in a future market design, industrial processes would be remunerated for providing reactive power. However, despite plans for a reactive power market, no asking prices are available in the literature yet. Thus, we perform a rough calculation based on current bilateral agreements, which range from 0.08 €/Mvarh to

Table 4
Quantification of the reactive power potential: The maximum and minimum reactive power (first two lines) are obtained from a nonlinear AC power flow simulation (Glücker et al., 2022), using the solved scheduling problem (10) as inputs. The reactive power potential (third line) is the difference between the momentary maximum and minimum reactive power.

	Minimum value	Maximum value	Average value
Maximum reactive power	41.2 Mvar	60.0 Mvar	49.8 Mvar
Minimum reactive power	−43.7 Mvar	−5.8 Mvar	−22.4 Mvar
Reactive power potential	47.9 Mvar	100.5 Mvar	72.2 Mvar

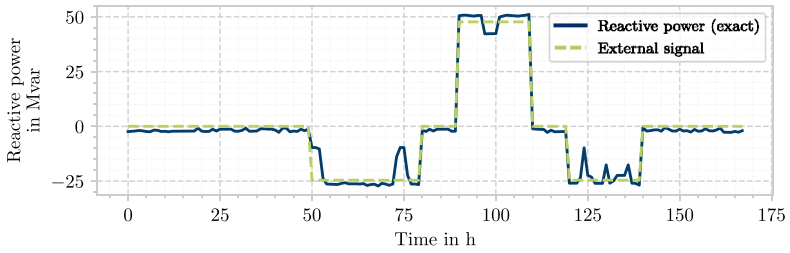

Fig. 8. Reactive power provision by following an external signal: The negative and positive values of the signal (dashed green line) are chosen based on the average minimum and maximum reactive power in Table 4.

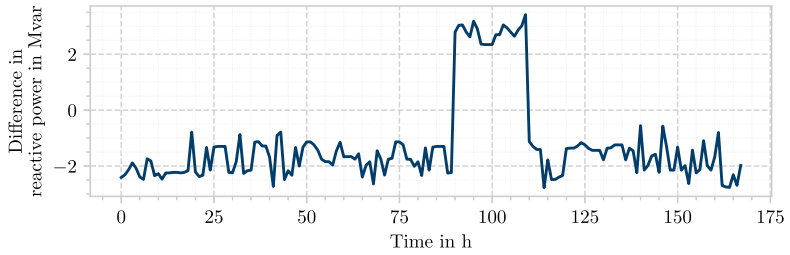

Fig. 9. Difference in reactive power at the PCC between the scheduling optimization model and the exact AC power flow equations. The schedule is identical to the one depicted in Fig. 8.

2.27 €/Mvarh (Bundesnetzagentur, 2018). Assuming the higher end of that range (2.27 €/Mvarh) and assuming that the process continuously provides its average minimum reactive power of −22.4 Mvar, (the requirement of capacitive reactive power exceeds that of inductive reactive power in Germany (Übertragungsnetzbetreiber, 2021)), the potential remuneration would amount to approximately 8.5 k€ per week, compared to electricity costs of 265 k€ per week. This rough calculation indicates the additional revenue potential for industrial processes that provide reactive power.

4.3. Reactive power provision by following an external signal

We now examine the provision of reactive power as an ancillary service. As publicly available information about plans for incorporating reactive power as a market-based ancillary service in Germany is very limited, we pragmatically assume that the industrial process plant will receive an external signal for reactive power provision. The reactive power signal might be based on local voltage measurements and applied within an automatic voltage-control scheme, coordinated by the TSO. As a specific illustrative case, we assume a signal that is piece-wise constant and has three possible values: zero, the average minimum reactive power of the copper production, and the average maximum reactive power of the copper production (cf. Table 4). The duration of the steps is determined by arbitrary choice but adheres to the chosen time discretization, i.e., the signal can only change its value at the time steps considered in the scheduling problem. To schedule the operations of the process such that the reactive power signal provided by the TSO can be tracked, we solve the optimization problem (12), i.e., we minimize the difference between the external signal and the reactive power at the PCC while ensuring maximum copper production and minimum electricity cost.

The resulting reactive power profiles of the process are depicted in Fig. 8. It can be seen that the signal can be followed quite closely most of the time, with few larger deviations. Specifically, deviations from the positive- or negative-valued external signal happen when tasks equipped with a power converter are operating at their maximum active power consumption, which limits the reactive power provision due to the maximum apparent power limit of the converters (cf. Eqs. (4a)–(4d)). Fig. 8 also shows slight deviations for reactive power target values of zero. We attribute these deviations to inaccuracies introduced by the regression model for approximating the AC power flow in the internal grid (cf. Section 2.2). Fig. 9 shows the difference between the true reactive power at the PCC, which is computed with the AC power flow equations, and the correction factor obtained from the regression model which is used for the scheduling. It can be observed that for a zero-valued or negative-valued signal, the difference is mostly negative, whereas for large positive-valued reactive power demand, differences are mostly positive.

4.4. Impact of reactive power provision on transmission grid

In the following section, we analyze the potential of industrial processes, such as the copper process presented, to enhance the voltage stability of the transmission grid by providing reactive power at the PCC. To conduct the analysis, we use the models of the German electricity system developed in prior work (Pesch, 2019), which include detailed representations of the European power market and the German transmission grid. The models, along with the necessary adaptations for this analysis, are outlined in Appendix E.

The scenario selected for the analysis describes a strong wind and high load hour as expected for the year 2025 (see Appendix B.3 in Pesch (2019)). In this critical use case, onshore and offshore wind turbines in northern and eastern Germany inject large amounts of electricity into the grid to supply a high power demand, mostly located in western and southern Germany. This results in some heavily loaded power lines along the north-south axes. In contrast to the original scenario, HVDC transmission lines, whose converter stations could significantly contribute to voltage stability, have been deactivated as they are not fully built and operational by 2025. The reactive power demand (from lines, transformers, and loads) is therefore covered by the conventional generation units operated in the grid.

Fig. 10 presents AC load flow calculations across three scenarios, each with different levels of reactive power provision from the copper process, to assess its voltage support potential.

In the base case (Fig. 10 (a) and (b)), the voltage conditions are analyzed without additional reactive power from industrial processes. The simulation results show notable voltage variations, with stable voltages in power generation areas (e.g., northern and eastern Germany) and significant voltage drops in areas with limited generation. Grid nodes within the marked area are particularly critical, as their voltage levels

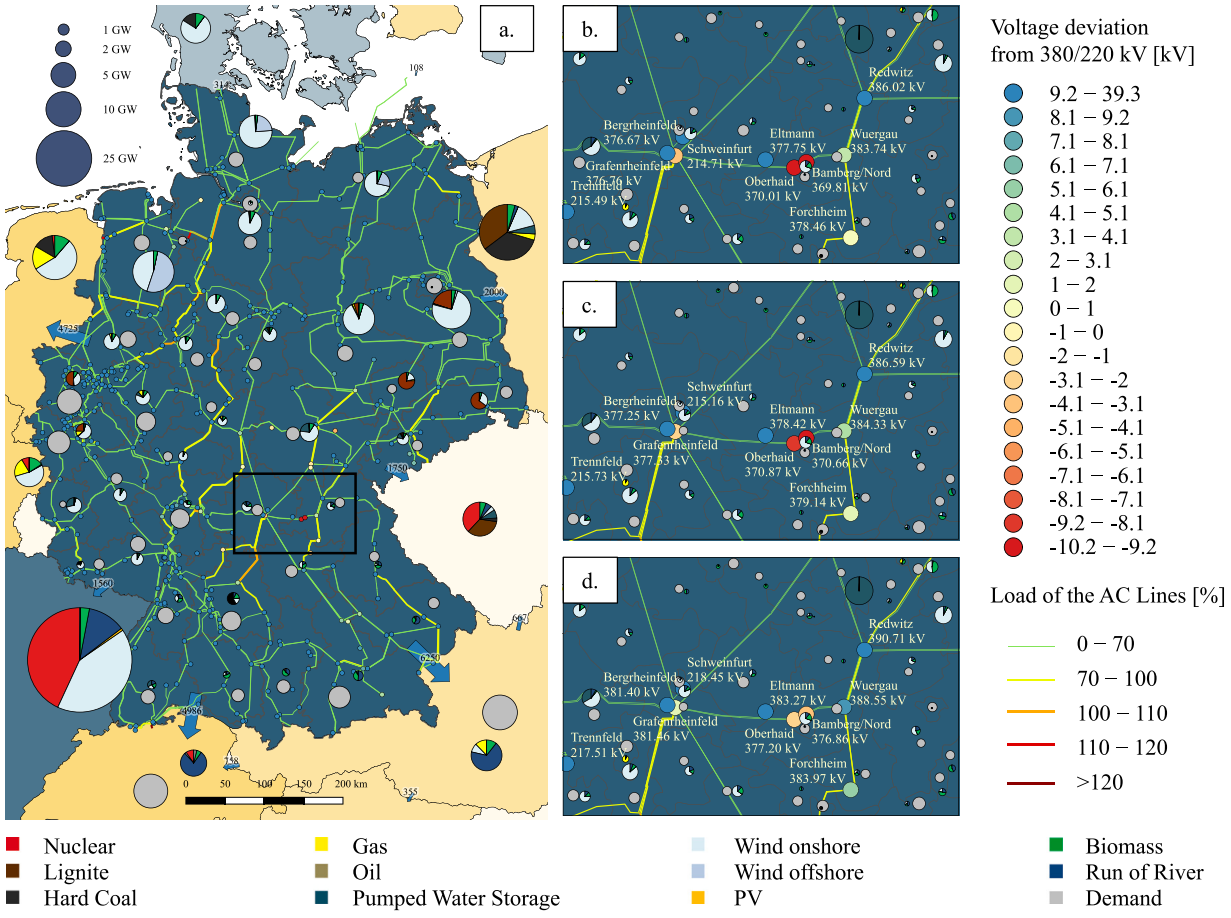

Fig. 10. Impact of varying reactive power provision on the voltage stability of the German transmission grid in a scenario with strong wind power feed-in and high load. Panel a. shows the load flow simulation for the base case without reactive power provision by industrial processes, while panel b. presents an excerpt of this scenario. Panel c. illustrates the effect of a 43.7 Mvar reactive power provision by an industrial process at the node Bamberg/Nord, and panel d. shows the impact of a 437 Mvar reactive power provision at the same node.

drop below the minimum permissible thresholds, thus indicating an unstable grid situation. As noted in Section 4.2, these nodes belong to the region *D25*, which requires additional controllable reactive power compensation of 1516 Mvar (Übertragungsnetzbetreiber, 2021). This highlights the need for additional measures to stabilize the grid, particularly in regions with high loads and limited local generation. Fig. 10 (c) depicts a scenario where an industrial process at the 110 kV node Bamberg/Nord provides up to 43.7 Mvar of reactive power, as derived in Section 4.2 for the copper process. The results show a slight improvement in voltage conditions, though the effect remains limited. A modest voltage increase is observed at surrounding nodes, but it is insufficient to bring voltages across the entire grid area within the permissible range. Finally, Fig. 10 (d) shows the impact of increasing reactive power provision at the 110 kV node Bamberg/Nord to 437 Mvar, assuming the availability of ten such industrial sites. This significant increase substantially improves the voltage conditions, raising the voltage at the critical node into the permissible range and stabilizing voltages at surrounding nodes.

This analysis demonstrates the potential of industrial processes to enhance grid stability by mitigating voltage issues through reactive power provision, provided sufficient capacity is available.

5. Discussion and limitations

With this first-of-its-kind integration of reactive power into process scheduling optimization, our study indicates a significant potential for power-intensive industrial production to aid local grid voltage stability. However, quite significant simplifications and assumptions had to be made in our study due to the lack of more detailed, publicly available data, a yet missing reactive power market for industrial power consumers, and the desire to obtain a computationally efficient linear formulation. In the following, we discuss the limitations of our assumptions and identify future possible research directions.

(1) We assumed fixed power factors for the electrical loads of tasks without a power converter to maintain a linear problem formulation. As the next step, the trade-off between model accuracy and computational complexity could be investigated by considering more realistic load models with variable power factors, see, e.g., Cresswell (2009), Perez Tellez (2017).

(2) We derived an internal power grid based on the voltage levels and active power consumed by the process tasks. Future studies should incorporate accurate information about the internal power grid and the installed equipment, most notably the power converters and their potential oversizing, which likely requires collaborations with industrial partners, ensuring a rigorous assessment.

(3) The planned implementation of a reactive power market (Netztransparenz.de, 2024; Bundesnetzagentur, 2024) will enable an assessment of remuneration and thus a better quantification of reactive power provision value. The additional revenue of reactive power provision could be considered along with revenues from offering demand response in a multi-market problem, see, e.g., Nolzen et al. (2022), Dalle Ave et al. (2019), Schäfer et al. (2019), Zhang et al. (2018), Glücker et al. (2025). In this context, the willingness of industrial stakeholders to participate in reactive power markets could be empirically assessed, considering factors such as remuneration, user-friendliness, and impact on their process operations.

Table 5
Electrical components and corresponding tasks in other power-intensive processes.

Process	Task	Main electrical component	Reference
Cement production	Limestone crushing	Electric motor/induction motor	Deolalkar (2021), Genç (2016)
	Raw meal milling	Electric motor/induction motor	Deolalkar (2021), Genç (2016)
	Raw meal blending	Compressor/blower	Deolalkar (2021)
	Raw meal preheating	Fan	Deolalkar (2021)
	Clinker cooling	Fan	Deolalkar (2021)
	Cement grinding	Electric motor/induction motor	Deolalkar (2021), Genç (2016)
Steel production	Electric arc furnace process	Electrodes (DC)	Pisciotta et al. (2022)
	Steel rolling	Electric motor	Singh and Singh (2023)
Pulp and paper production	Kraft pulp mill process	Electric motor[a]	Nilsson et al. (1995)

[a] For pumps, fans, compressors and mixers.

(4) We suggested, as a first approach, a linear approximation of the internal power flow in addition to the LinDistFlow equations to ensure computational efficiency while considering the reactive power losses within the internal grid. Future research could explore iterative approaches between (i) scheduling optimization with a (linear) approximation of the AC power flow and (ii) AC power flow simulations, until a defined convergence is reached. This iterative optimization formulation could enable computationally efficient scheduling and ensure the preciseness of the achievable reactive power.

(5) We considered the copper production process as an industrial case study to show the reactive power potential of a power-intensive industrial production process. Future work could extend the presented methodology to assess the reactive power potential of other industrial production processes. As a possible starting point, a non-exhaustive list of major power-intensive production processes, i.e., cement, steel and paper production, with important tasks and electrical components can be found in Table 5. In particular, the overview considers important tasks and their functionality from an electrical perspective, which allows to derive power factor assumptions for future investigation.

6. Conclusion and future research

We present an approach for integrating reactive power into process scheduling optimization, which allows us to determine a first estimate of the reactive power potential of a specific power-intensive process. To this end, we adapt our previous demand response scheduling formulation (Röben et al., 2022) to include the reactive power of key electricity-driven process tasks as well as the internal power grid. In particular, we include tasks that are equipped with local power converters that can adjust their reactive power and thus constitute an important lever in reactive power provision.

As we demonstrate by the example of the copper production, conventional demand response scheduling neglecting reactive power risks that the power factor at the point of common coupling (PCC) occasionally drops below the current regulatory limit in Germany. This finding shows that consideration of reactive power is important when shifting load. Our investigation of the achievable reactive power at the PCC indicates a significant reactive power potential that can be accessed without sacrificing the overall copper production volume and the electricity cost of the process. This result suggests a significant potential for the copper production to provide reactive power. Assuming that the provision of reactive power as an ancillary service would require the ability to follow an external signal, we show that the scheduling optimization can do so and produces only relatively small tracking errors. We further demonstrate by means of a simulation model that large industrial processes providing reactive power could alleviate voltage problems in the German transmission grid.

For future research, we identify five possible directions: (1) advancing the modeling detail with regard to reactive power, (2) determining incentives and remunerations for the industry to provide reactive power, (3) understanding future requirements of reactive power from the perspective of the transmission system operator (TSO), (4) enabling provision of reactive power by computationally efficient real-time scheduling, and (5) analyzing the reactive power potential of other major industrial processes.

Author contribution

- PG and SG jointly conceptualized the work, conducted the primary investigations, executed the programming work, carried out the analysis, and co-authored the manuscript.
- PG wrote the electrical engineering related parts of Sections 2.1 and 2.2, developed the estimation of reactive power losses (cf. Section 2.2), derived the power factor assumptions (cf. Section 3.1), derived the local power grid of the copper process (cf. Section 3.2), and had the lead in implementing respective code and writing of the respective sections, all with continuous feedback from SG.
- SG extended the RTN model (cf. Section 3.1), set up the three scheduling problems (cf. Section 2.3), and had the lead in implementing respective code and writing of the respective sections, all with continuous feedback from PG.
- AO supported the investigation by curating data of the electricity-consuming tasks of the copper process (cf. Sections 3.1 and 3.2) and identifying tasks in other power-intensive processes (cf. Section 6).
- TP conceptualized and carried out the analysis in Section 4.4.
- AB, TP and MD supervised the conceptualization process.
- MD supervised the writing process.
- All authors reviewed and edited the manuscript.

CRediT authorship contribution statement

Philipp Glücker: Conceptualization, Data curation, Formal analysis, Investigation, Methodology, Project administration, Software, Validation, Visualization, Writing – original draft. **Sonja H.M. Germscheid:** Conceptualization, Formal analysis, Investigation, Methodology, Project administration, Software, Writing – original draft. **Ariana Y. Ojeda-Paredes:** Data curation, Investigation, Writing – review & editing. **Andrea Benigni:** Funding acquisition, Supervision, Writing – review & editing. **Manuel Dahmen:** Funding acquisition, Supervision, Writing – review & editing. **Thiemo Pesch:** Conceptualization, Funding acquisition, Supervision, Writing – review & editing.

Declaration of competing interest

The authors declare that they have no known competing financial interests or personal relationships that could have appeared to influence the work reported in this paper.

Acknowledgments

This work was supported by the Helmholtz Association in the context of the Innovation Pool project “Energy Transition and Circular Economy”.

Table A.1
Line parameters of the internal grid: The line parameters account for the point of common coupling (PCC), the smelting offgas handling (SOH), the converter offgas handling (COH), the anode furnace offgas handling (AFOH), the air separation unit (ASU), the slag cleaning furnace (SCF), the air compressor (AC), and the electrolytic refining (EF). Electric buses at the respective voltage level are considered, e.g., Bus 20 kV, as well as buses that are connected to a task via an additional transformer for a lower voltage level, e.g., Bus EF for the electrolytic refining. The transformers and cables are characterized by the maximum apparent power $\bar{S}_{nk}$, the resistance R_{nk}, the reactance X_{nk}, and the capacitance C_{nk}.

Electric bus n (from)		Electric bus k (to)						
Bus name	Voltage level	Bus name	Voltage level	Type	$\bar{S}_{nk}$	R_{nk} [Ω]	X_{nk} [Ω]	C_{nk} [nF]
Bus PCC	110 kV	Bus 20 kV	20 kV	Transformer	63 MVA	8×10^{-5}	0.0045	0
Bus PCC	110 kV	Bus 10 kV	10 kV	Transformer	63 MVA	8×10^{-5}	0.0045	0
Bus 20 kV	20 kV	SOH	20 kV	Cable	26 MVA	0.025	0.046	400
Bus 20 kV	20 kV	COH	20 kV	Cable	23.5 MVA	0.019	0.034	1200
Bus 10 kV	10 kV	Bus AFOH	10 kV	Cable	8.15 MVA	0.15	0.3	561
Bus AFOH	10 kV	AFOH	0.4 kV	Transformer	2.5 MVA	0.428	1.529	0
Bus 10 kV	10 kV	ASU	10 kV	Cable	16.3 MVA	0.025	0.05	187
Bus 10 kV	10 kV	AC	10 kV	Cable	8.15 MVA	0.05	0.1	187
Bus 10 kV	10 kV	Bus SCF	10 kV	Cable	8.15 MVA	0.025	0.05	187
Bus SCF	10 kV	SCF	0.4 kV	Transformer	3.8 MVA	0.286	1.019	0
Bus 10 kV	10 kV	Bus EF	10 kV	Cable	32.5 MVA	0.025	0.0125	748
Bus EF	10 kV	EF	0.1 kV	Transformer	18.9 MVA	0.0857	0.306	0

Appendix A. Internal power grid

The values for the electrical parameters of the internal power grid are listed in Table A.1.

Appendix B. Scheduling optimization neglecting reactive power

In Section 4.1 of the main text, we discuss the scheduling optimization neglecting reactive power. In particular, we show that for certain time steps, the power factor drops below 0.95. Fig. B.1 shows the individual task operation over the respective scheduling horizon. Time steps with a power factor below 0.95 correspond to time steps during which only the slag cleaning task with its power factor of 0.93 is operating.

Appendix C. Reactive power potential

In Section 4.2 of the main text, we discuss the reactive power potential, i.e., the difference between the minimum and maximum achievable reactive power. Our results suggest that the minimum and maximum reactive power optimizations lead to slightly different schedules, i.e., slightly different momentary consumption of active power. Fig. C.1 shows the task operation over the scheduling horizon for both schedules in detail and confirms that the process operations are slightly different.

Appendix D. Accuracy of linear heuristic

In Section 4.2 of the main text, we identify the reactive power potential of the industrial process by maximizing and minimizing the reactive power at the PCC. The presented results are based on an *ex-post* nonlinear power flow simulation which takes the exact AC OPF equations into account. Fig. D.1 presents the difference between LinDistFlow, the linear approximation model, and the exact AC OPF equations. The results show that the linear approximation significantly reduces the reactive power deviation from the nonlinear AC OPF approach compared to LinDistFlow.

Appendix E. Modeling of the European power market and the German transmission grid with the integration of the reactive power potential of industrial processes

The employed power market model developed in Pesch (2019) considers dispatch planning on several time scales: from a one-year planning period for revisions to day-ahead optimization, which determines the balance of electricity generation, consumption and the use of flexibility options on an hourly basis. Technical constraints such as minimum and maximum up and down times, part-load efficiencies, start-up processes and the provision of balancing capacity are taken into account. The employed transmission grid model developed in Pesch (2019) represents the German high and extra-high voltage grid (110 – 380 kV) and is based on real grid data provided by the German Federal Network Agency (Bundesnetzagentur), which has also been used for the official German Grid Development Plan (Übertragungsnetzbetreiber, 2012). Since the original purpose of the model was to determine the grid expansion requirements based on current-related rather than voltage-related criteria, fictive reactive power compensation was modeled throughout the entire German transmission grid (cf. Übertragungsnetzbetreiber (2012)). However, for the analysis in this paper, these compensations were limited to the boundaries required for the convergence of the model, allowing voltage differences to be observed across the different scenarios. The integration of the flexible reactive power provision of the industrial process into the transmission grid model is depicted in Fig. E1. The reactive power provision of the industrial process plant Q must be within the maximum reactive power value $Q_{\max}$ and the minimum reactive power value $Q_{\min}$ as identified in Table 4. It is integrated as an external ward with the equivalent reactance X_{eq} and no active power, while its voltage magnitude $|U_{\text{eq}}|$ must be within its upper operating limit of 121 kV that is assumed for 110 kV nodes.

Data availability

Data will be made available on request.

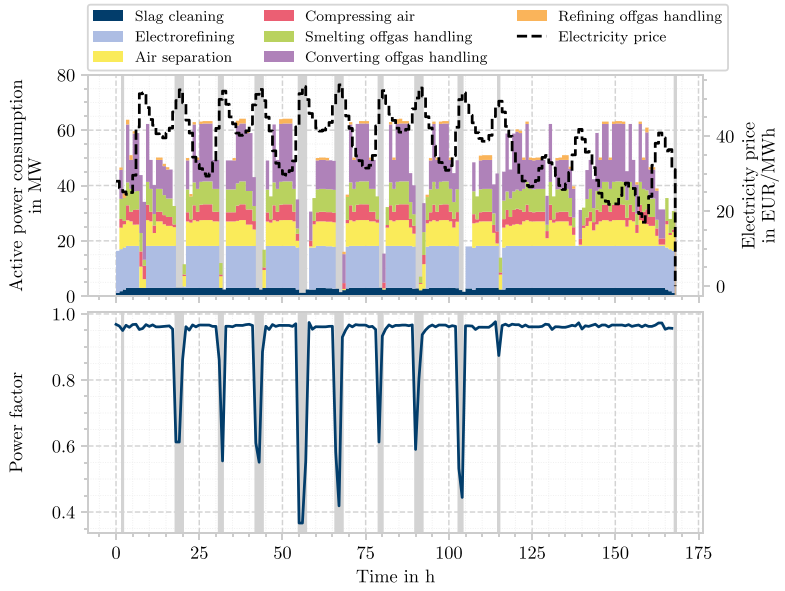

Fig. B.1. Detailed results for scheduling that neglects the reactive power (cf. Section 4.1 of the main text) (top) and corresponding power factor of the entire process (bottom). The gray areas indicate violations of the current German grid connection requirement that states that the power factor at the PCC must not fall below 0.95 (Bundesnetzagentur, 2018).

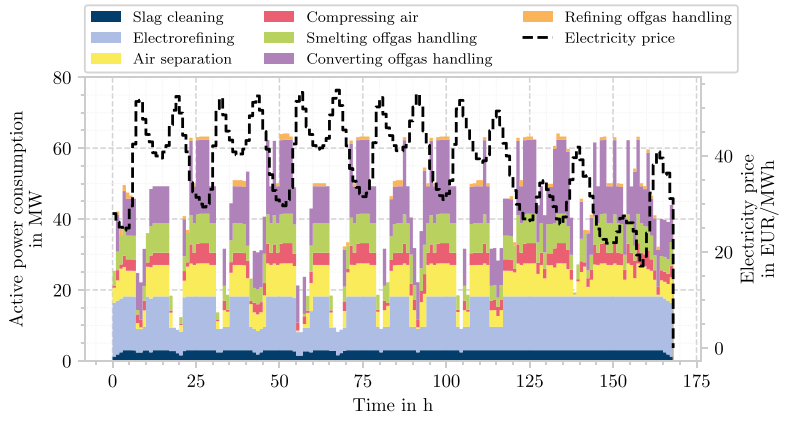

(a)

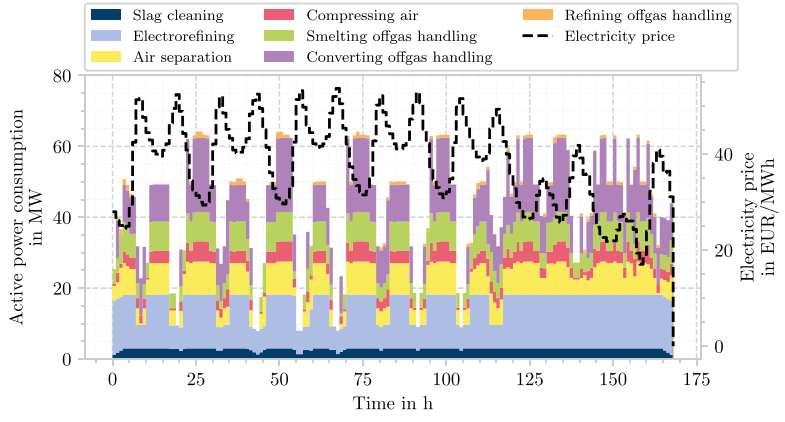

(b)

Fig. C.1. Detailed scheduling results for maximization (top) and minimization (bottom) of reactive power (cf. Section 4.2 of the main text).

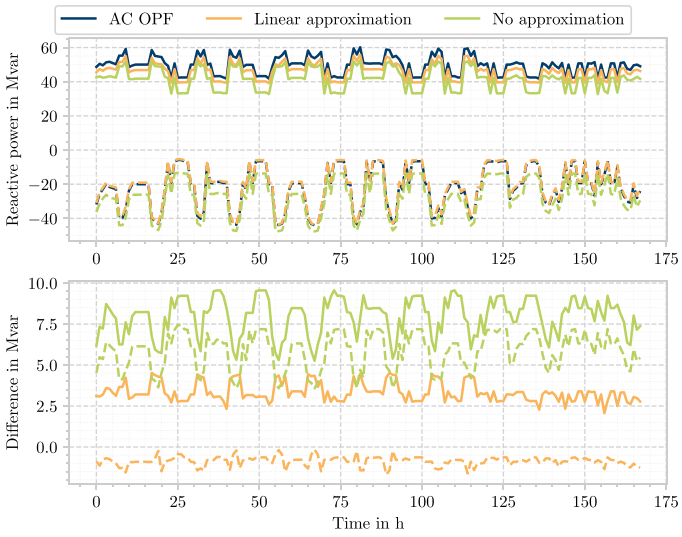

Fig. D.1. Reactive power and difference between exact nonlinear simulation (AC OPF), LinDistFlow with the linear approximation (Linear approximation), and LinDistFlow without an additional approximation (No approximation). The solid lines represent maximum reactive power schedules, and the dashed lines represent minimum reactive power schedules.

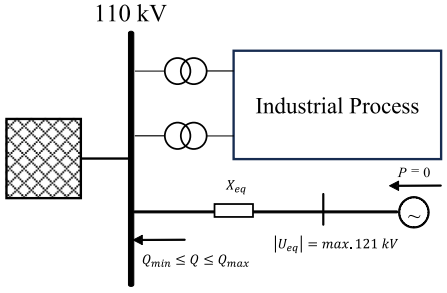

Fig. E1. Modeling of the reactive power provision by the industrial process at the point of common coupling.

References

Abeysinghe, S., Wu, J., Sooriyabandara, M., Abeysekera, M., Xu, T., Wang, C., 2018. Topological properties of medium voltage electricity distribution networks. Appl. Energy 210, 1101–1112. http://dx.doi.org/10.1016/j.apenergy.2017.06.113.

Akagi, H., Watanable, E.H., Aredes, M., 2017. Instantaneous Power Theory and Applications to Power Conditioning, second ed. Wiley-IEEE Press.

Albadi, M., El-Saadany, E., 2008. A summary of demand response in electricity markets. Electr. Power Syst. Res. 78 (11), 1989–1996. http://dx.doi.org/10.1016/j.epsr.2008.04.002.

Aneke, M., Wang, M., 2015. Potential for improving the energy efficiency of cryogenic air separation unit (ASU) using binary heat recovery cycles. Appl. Therm. Eng. 81, 223–231. http://dx.doi.org/10.1016/j.applthermaleng.2015.02.034.

Ausfelder, F., Seitz, A., 2018. Flexibilitätsoptionen in der Grundstoffindustrie : Methodik, Potenziale, Hemmnisse. DECHEMA.

Bahl, B., Kümpel, A., Seele, H., Lampe, M., Bardow, A., 2017. Time-series aggregation for synthesis problems by bounding error in the objective function. Energy 135, 900–912. http://dx.doi.org/10.1016/j.energy.2017.06.082.

Baradar, M., Hesamzadeh, M.R., Ghandhari, M., 2013. Second-order cone programming for optimal power flow in VSC-type AC-DC grids. IEEE Trans. Power Syst. 28 (4), 4282–4291. http://dx.doi.org/10.1109/TPWRS.2013.2271871.

Barbosa-Póvoa, A., Pantelides, C., 1997. Design of multipurpose plants using the resource-task network unified framework. Comput. Chem. Eng. 21, 703–708. http://dx.doi.org/10.1016/S0098-1354(97)87585-0, Supplement to Computers and Chemical Engineering.

Barker, I.J., Stewart, A.B., 1980. Inductive reactance, and the operation of large submerged-arc furnaces. J. South Afr. Inst. Min. Met. 123–128.

Baumgärtner, N., Delorme, R., Hennen, M., Bardow, A., 2019. Design of low-carbon utility systems: Exploiting time-dependent grid emissions for climate-friendly demand-side management. Appl. Energy 247 (April), 755–765. http://dx.doi.org/10.1016/j.apenergy.2019.04.029.

Blumberg, G., Wagner, C., Lehnert, W., Bucksteeg, M., Greve, M., 2021. Marktgestützte Beschaffung von Blindleistung. Tech. rep., Federal Ministry for Economic Affairs and Climate Action, Germany, URL https://www.bmwk.de/Redaktion/DE/Publikationen/Energie/ergebnispapier-beschaffung-von-blindleistung.html. (Accessed 04 November 2023).

Bohlayer, M., Fleschutz, M., Braun, M., Zöttl, G., 2020. Energy-intense production-inventory planning with participation in sequential energy markets. Appl. Energy 258, 113954. http://dx.doi.org/10.1016/j.apenergy.2019.113954.

Bundesnetzagentur, 2018. Diskussionspapier - Blindleistungsbereitstellung für den Netzbetrieb. URL https://www.bundesnetzagentur.de/SharedDocs/Downloads/DE/Sachgebiete/Energie/Unternehmen_Institutionen/NetzentwicklungUndSmartGrid/SmartGrid/Blindleistungspapier.html. (Accessed 04 June 2024).

Bundesnetzagentur, 2024. Beschaffungskonzept für die Spezifikationen und technischen Anforderungen der transparenten, diskriminierungsfreien und marktgestützten Beschaffung der nicht frequenzgebundenen Systemdienstleistung 'Dienstleistungen zur Spannungsregelung' ('Blindleistung') gem. §12h Abs. 1 S. 1 Nr. 1, Abs. 5 EnWG. available under https://www.bundesnetzagentur.de/DE/Beschlusskammern/1_GZ/BK6-GZ/2023/BK6-23-072/BK6-23-072_beschaffungskonzept.pdf?_blob=publicationFile&v=4. (Accessed 27 September 2024).

Burre, J., Bongartz, D., Brée, L., Roh, K., Mitsos, A., 2020. Power-to-X: Between electricity storage, e-production, and demand side management. Chem. Ing. Tech. 92 (1–2), 74–84. http://dx.doi.org/10.1002/cite.201900102.

Castro, P.M., Barbosa-Póvoa, A.P., Novais, A.Q., 2005. Simultaneous design and scheduling of multipurpose plants using resource task network based continuous-time formulations. Ind. Eng. Chem. Res. 44 (2), 343–357. http://dx.doi.org/10.1021/ie049817h.

Castro, P.M., Harjunkoski, I., Grossmann, I.E., 2009. New Continuous-Time Scheduling Formulation for Continuous Plants under Variable Electricity Cost. Ind. Eng. Chem. Res. 48 (14), 6701–6714.

Castro, P.M., Sun, L., Harjunkoski, I., 2013. Resource–task network formulations for industrial demand side management of a steel plant. Ind. Eng. Chem. Res. 52, 13046–13058.

Cresswell, C., 2009. Steady State Load Models for Power System Analysis (Ph.D. thesis). University of Edinburgh.

Dalle Ave, G., Harjunkoski, I., Engell, S., 2019. A non-uniform grid approach for scheduling considering electricity load tracking and future load prediction. Comput. Chem. Eng. 129, 106506. http://dx.doi.org/10.1016/j.compchemeng.2019.06.031.

Daryanian, B., Bohn, R., Tabors, R., 1989. Optimal demand-side response to electricity spot prices for storage-type customers. IEEE Trans. Power Syst. 4 (3), 897–903. http://dx.doi.org/10.1109/59.32577.

Deolalkar, S., 2021. Handbook for Designing Cement Plants, second ed. Bsp Books Pvt. Limited.

Deutsche Energie-Agentur GmbH (dena) and TU Dortmund and ef.Ruhr GmbH, 2014. dena-Studie Systemdienstleistungen 2030 - Sicherheit und Zuverlässigkeit einer Stromversorgung mit hohem Anteil erneuerbarer Energien. Tech. rep., Berlin, URL https://www.dena.de/fileadmin/dena/Dokumente/Pdf/9094_dena-Studie_Systemdienstleistungen_2030.pdf. (Accessed 23 March 2021).

Eicke, A., Ruhnau, O., Hirth, L., 2021. Electricity balancing as a market equilibrium: An instrument-based estimation of supply and demand for imbalance energy. Energy Econ. 102, 105455. http://dx.doi.org/10.1016/j.eneco.2021.105455.

European Commission, 2022. New continuous smelting and refining process for copper. online, URL https://cordis.europa.eu/project/id/EE.-00251-80. (Accessed 30 August 2023).

Federal Ministry for Economic Affairs and Climate Action Germany, 2023. Roadmap Systemstabilität. Tech. rep., Berlin, URL https://www.bmwk.de/Redaktion/DE/Dossier/roadmap-systemstabilitaet.html. (Accessed 22 October 2023).

Finch, J.W., Giaouris, D., 2008. Controlled AC electrical drives. IEEE Trans. Ind. Electron. 55 (2), 481–491. http://dx.doi.org/10.1109/TIE.2007.911209.

Forum Netztechnik/Netzbetrieb im VDE (FNN), 2013. Versorgungszuverlässigkeit und Spannungsqualität in Deutschland. Tech. rep., VDE Verband der Elektrotechnik Elektronik Informationstechnik, URL https://www.vde.com/resource/blob/824912/2a9a511f3dd6da0e5c00dab2d4db4398/fnn-fakten-versorgungsqualitaet-2013-03-11-data.pdf. (Accessed 11 August 2024).

Frank, S., Rebennack, S., 2016. An introduction to optimal power flow: Theory, formulation, and examples. IIE Trans. 48 (12), 1172–1197. http://dx.doi.org/10.1080/0740817X.2016.1189626.

Gao, X., Zhou, D., Anvari-Moghaddam, A., Blaabjerg, F., 2021. Grid-following and grid-forming control in power electronic based power systems: A comparative study. In: IECON 2021 – 47th Annual Conference of the IEEE Industrial Electronics Society. pp. 1–6. http://dx.doi.org/10.1109/IECON48115.2021.9589432.

Genç, Ö., 2016. Energy-efficient technologies in cement grinding. In: Yilmaz, S., Ozmen, H.B. (Eds.), High Performance Concrete Technology and Applications. IntechOpen, Rijeka, pp. 115–116. http://dx.doi.org/10.5772/64427.

Germscheid, S.H., Röben, F.T., Sun, H., Bardow, A., Mitsos, A., Dahmen, M., 2023. Demand response scheduling of copper production under short-term electricity price uncertainty. Comput. Chem. Eng. 178, 108394. http://dx.doi.org/10.1016/j.compchemeng.2023.108394.

Gesamtkonsortium NEW 4.0 , 2021. NEW 4.0 Synthesebericht. Tech. rep., Norddeutsche Energiewende, URL http://www.new4-0.de/ergebnisse/. (Accessed 08 May 2023).

Gesamtkonsortium NEW 4.0, 2021. ANNEX - Anhang zur Ergebnissynthese von NEW 4.0. Tech. rep., Norddeutsche Energiewende, URL https://www.new4-0.de/wp-content/uploads/2021/04/20210325-NEW4-0-Synthesebericht-Annex-WEB-1.pdf. (Accessed 08 May 2023).

Glover, J.D., Overbye, T.J., Sarma, M.S., 2017. Power System Analysis & Design, sixth ed. Cengage Learning.

Glücker, P., Langiu, M., Pesch, T., Dahmen, M., Benigni, A., 2022. Incorporating AC Power Flow into the Multi-Energy System Optimization Framework COMANDO. In: 2022 Open Source Modelling and Simulation of Energy Systems. OSMSES, pp. 1–6. http://dx.doi.org/10.1109/OSMSES54027.2022.9769138.

Glücker, P., Mhanna, S., Pesch, T., Mancarella, P., Benigni, A., 2025. Optimal design of local multi-energy systems: Impact of reactive power provision. In: 2025 IEEE PES Innovative Smart Grid Technologies Conference Europe (ISGT Europe). pp. 1–5. http://dx.doi.org/10.1109/ISGTEurope64741.2025.11305385.

Gurobi Optimization, LLC, 2024. Gurobi optimizer reference manual.

König, R., Weyer, A., Degel, R., Schmidl, J., Kadereit, H., Specht, A., 2016. Highly efficient slag cleaning — latest results from pilot-scale tests. In: REWAS 2013: Enabling Materials Resource Sustainability. Springer International Publishing, pp. 2–12. http://dx.doi.org/10.1007/978-3-319-48763-2_1.

Koponen, J., Poluektov, A., Ruuskanen, V., Kosonen, A., Niemelä, M., Ahola, J., 2021. Comparison of thyristor and insulated-gate bipolar transistor -based power supply topologies in industrial water electrolysis applications. J. Power Sources 491, 229443. http://dx.doi.org/10.1016/j.jpowsour.2020.229443.

Kromer, B., Golubev, D., 2023. Air separation plants: Flexibilisation of air separation plants. Summer School Enabling the Transition to a New Energy System.

Kroposki, B., Pink, C., DeBlasio, R., Thomas, H., Simões, M., Sen, P.K., 2010. Benefits of power electronic interfaces for distributed energy systems. IEEE Trans. Energy Convers. 25 (3), 901–908. http://dx.doi.org/10.1109/TEC.2010.2053975.

Love, D.J., 1993. Reliability of utility supply configuration for industrial power systems. In: Conference Record of the 1993 IEEE Industry Applications Conference Twenty-Eighth IAS Annual Meeting, vol. 2, pp. 1469–1474. http://dx.doi.org/10.1109/IAS.1993.299195.

Low, S.H., 2014. Convex relaxation of optimal power flow—Part I: Formulations and equivalence. IEEE Trans. Control. Netw. Syst. 1 (1), 15–27. http://dx.doi.org/10.1109/TCNS.2014.2309732.

Mirafzal, B., Adib, A., 2020. On grid-interactive smart inverters: Features and advancements. IEEE Access 8, 160526–160536. http://dx.doi.org/10.1109/ACCESS.2020.3020965, Conference Name: IEEE Access.

Mitsos, A., Asprion, N., Floudas, C.A., Bortz, M., Baldea, M., Bonvin, D., Caspari, A., Schäfer, P., 2018. Challenges in process optimization for new feedstocks and energy sources. Comput. Chem. Eng. 113, 209–221. http://dx.doi.org/10.1016/j.compchemeng.2018.03.013.

Mohan, N., Undeland, T.M., Robbins, W.P., 2002. Power Electronics: Converters, Applications and Design. John Wiley & Sons Inc.

Moore, J.C., 1974. Electric motors for centrifugal compressor drives. In: Proceedings of the 3rd Turbomachinery Symposium.

Naughton, J.C., 2022. A Modelling Framework for Virtual Power Plants Under Uncertainty (Ph.D. thesis). University of Birmingham.

Naughton, J., Wang, H., Cantoni, M., Mancarella, P., 2021. Co-optimizing virtual power plant services under uncertainty: A robust scheduling and receding horizon dispatch approach. IEEE Trans. Power Syst. 36 (5), 3960–3972. http://dx.doi.org/10.1109/TPWRS.2021.3062582.

Netztransparenz.de, 2024. Blindleistung - Einheitliche Auslegung von E-STATCOM. available under https://www.netztransparenz.de/de-de/Systemdienstleistungen/Spannungshaltung/Blindleistung. (Accessed 27 September 2024).

Next Kraftwerke, 2023. Was ist der Strommarkt?. URL https://www.next-kraftwerke.de/wissen/strommarkt. (Accessed 24 February 2023).

Nilsson, L., Larson, E., Subbiah, A., 1995. Energy analysis of a kraft pulp mill: Potential for energy efficiency and advanced biomass cogeneration. National Ind. Energy Technol. Conf. 17, 232–246.

Nolzen, N., Ganter, A., Baumgärtner, N., Leenders, L., Bardow, A., 2022. Where to market flexibility? Optimal participation of industrial energy systems in balancing-power, day-ahead, and continuous intraday electricity markets. arXiv: 2212.12507, arXiv:2212.12507.

Oeding, D., Oswald, B.R., 2016. Elektrische Kraftwerke und Netze. Springer Berlin Heidelberg, http://dx.doi.org/10.1007/978-3-662-52703-0.

Pantelides, C.C., 1994. Unified frameworks for optimal process planning and scheduling. In: Proceedings on the Second Conference on Foundations of Computer Aided Operations. Cache Publications New York, pp. 253–274.

Peñalvo-López, E., León-Martínez, V., Montañana-Romeu, J., Cárcel-Carrasco, J., 2021. Passive reactive power compensators for improving the sustainability of three-phase, four-wire sinusoidal systems supplied by unbalanced voltages. Sustainability 13 (20), http://dx.doi.org/10.3390/su132011134.

Perez Tellez, A., 2017. Modelling Aggregate Loads in Power Systems (Ph.D. thesis). KTH Stockholm.

Pesch, T., 2019. Multiscale modelling of integrated energy and electricity systems. In: Schriften des Forschungszentrums Jülich. Energie & Umwelt / Energy & Environment, vol. 485, Verlag des Forschungszentrums Jülich, Jülich, http://dx.doi.org/10.18154/RWTH-2020-00990, 1 Online–Ressource (XXV, 384 Seiten) : Illustrationen, Diagramme, Karten, Dissertation, RWTH Aachen University, 2019.

Pisciotta, M., Pilorgé, H., Feldmann, J., Jacobson, R., Davids, J., Swett, S., Sasso, Z., Wilcox, J., 2022. Current state of industrial heating and opportunities for decarbonization. Prog. Energy Combust. Sci. 91, 100982. http://dx.doi.org/10.1016/j.pecs.2021.100982.

Plößer, T., 2021. Potenzial und Auswirkung von Blindleistungsbereitstellung durch flexible Industrieanlagen in Verteilnetzen (Ph.D. thesis). TU Darmstadt.

Rauch, J., Brückl, O., 2023. Achieving optimal reactive power compensation in distribution grids by using industrial compensation systems. Electricity 4 (1), 78–95. http://dx.doi.org/10.3390/electricity4010006, URL https://www.mdpi.com/2673-4826/4/1/6.

Röben, F.T., Liu, D., Reuter, M.A., Dahmen, M., Bardow, A., 2022. The demand response potential in copper production. J. Clean. Prod. 362, 132221. http://dx.doi.org/10.1016/j.jclepro.2022.132221.

Ruuskanen, V., Koponen, J., Kosonen, A., Niemelä, M., Ahola, J., Hämäläinen, A., 2020. Power quality and reactive power of water electrolyzers supplied with thyristor converters. J. Power Sources 459, 228075. http://dx.doi.org/10.1016/j.jpowsour.2020.228075, URL https://www.sciencedirect.com/science/article/pii/S0378775320303785.

Saadat, H., 1999. Power System Analysis. McGraw Hill.

Schäfer, P., Westerholt, H.G., Schweidtmann, A.M., Ilieva, S., Mitsos, A., 2019. Model-based bidding strategies on the primary balancing market for energy-intense processes. Comput. Chem. Eng. 120, 4–14. http://dx.doi.org/10.1016/j.compchemeng.2018.09.026.

Schlesinger, M.E., King, M.J., Sole, K.C., Davenport, W.G., 2011. Extractive Metallurgy of Copper. Elsevier, http://dx.doi.org/10.1016/B978-0-08-096789-9.10001-0.

Seabold, S., Perktold, J., 2010. Statsmodels: Econometric and statistical modeling with python. In: 9th Python in Science Conference.

Singh, G., Singh, P.K., 2023. Reduction of energy and fuel consumption in the hot-rolling steel sector. Clean. Eng. Technol. 17, 100689. http://dx.doi.org/10.1016/j.clet.2023.100689.

Singh, B., Singh, B., Chandra, A., Al-Haddad, K., Pandey, A., Kothari, D., 2004. A review of three-phase improved power quality AC-DC converters. IEEE Trans. Ind. Electron. 51 (3), 641–660. http://dx.doi.org/10.1109/TIE.2004.825341.

Straits Research, 2024. Electric drives market size & outlook, 2024–2032.

Thurner, L., Scheidler, A., Schafer, F., Menke, J.H., Dollichon, J., Meier, F., Meinecke, S., Braun, M., 2018. pandapower - an open source python tool for convenient modeling, analysis and optimization of electric power systems. IEEE Trans. Power Syst. http://dx.doi.org/10.1109/TPWRS.2018.2829021.

Turner, J.H., Lawless, P.A., Yamamoto, T., Coy, D.W., Greiner, G.P., McKenna, J.D., Vatavuk, W.M., 1988. Sizing and costing of electrostatic precipitators. JAPCA 38 (4), 458–471. http://dx.doi.org/10.1080/08940630.1988.10466396, arXiv:https://doi.org/10.1080/08940630.1988.10466396.

Übertragungsnetzbetreiber, 2012. Netzentwicklungsplan strom 2012.

Übertragungsnetzbetreiber, 2021. Netzentwicklungsplan Strom 2035, Systemstabilität, zweiter Entwurf. Tech. rep., p. 228.

Unified Facilities Guide Specifications (UFGS), 2020. Division 43 - process gas and liquid handling, purification and storage equipment. SECTION 43 11 00.10 off-gas fans, blowers and pumps. URL https://www.wbdg.org/FFC/DOD/UFGS/UFGS%2043%2011%2000.10.pdf. (Accessed 30 October 2023).

Vardakas, J.S., Zorba, N., Verikoukis, C.V., 2015. A survey on demand response programs in smart grids: Pricing methods and optimization algorithms. IEEE Commun. Surv. Tutorials 17 (1), 152–178. http://dx.doi.org/10.1109/COMST.2014.2341586.

VEM Motors Finland, 2021. https://www.vem.fi/en/news/expansion-of-our-turbo-compressor-motors/. (Accessed 12 December 2023).

Wolgast, T., Ferenz, S., Nieße, A., 2022. Reactive power markets: A review. IEEE Access 10, 28397–28410. http://dx.doi.org/10.1109/ACCESS.2022.3141235.

Zhang, Q., Bremen, A.M., Grossmann, I.E., Pinto, J.M., 2018. Long-term electricity procurement for large industrial consumers under uncertainty. Ind. Eng. Chem. Res. 57, 3333–3347. http://dx.doi.org/10.1021/acs.iecr.7b04589.

Zhang, Q., Grossmann, I.E., 2016. Planning and scheduling for industrial demand side management: Advances and challenges. In: Alternative Energy Sources and Technologies. Springer International Publishing, pp. 383–414. http://dx.doi.org/10.1007/978-3-319-28752-2_14.

Zhong, J., Bhattacharya, K., 2002. Toward a competitive market for reactive power. IEEE Trans. Power Syst. 17 (4), 1206–1215. http://dx.doi.org/10.1109/TPWRS.2002.805025.